Preprints of the 21st IFAC World Congress (Virtual)
Berlin, Germany, July 12-17, 2020

Comparison of Optical and Ultrasonic Methods for Quantification of Underwater Gas Leaks [1]

Rogério Y. Takimoto [*,2] **Marcelo Y. Matuda** [**,3]
Timóteo F. Oliveira [**,4] **Julio C. Adamowski** [**,5]
André K. Sato [*,6] **Thiago C. Martins** [*,7]
Marcos S. G. Tsuzuki [*,8]

[*] *Laboratory of Computational Geometry*
[**] *Laboratory of Sensors and Actuators*
Mechatronics and Mechanical Systems Engineering Department,
Escola Politécnica da Universidade de São Paulo, São Paulo, Brazil

Abstract: The quantification of underwater gas leakage using optical and ultrasound technologies is presented. In the optical method, a high-speed camera is utilized, and the captured images are processed with segmentation techniques. The bubble is considered as an ellipsoid and its projected largest diameter is determined. The case of bubbles partial overlapping is also processed. In the ultrasound method, a ultrasonic linear array is used to capture images. For both methods, vertical speed, size of the bubbles, the bubble emission rate and the leak rate are measured. The results of the optical and acoustic methods are compared and analyzed.

Keywords: Image Processing, Bubble detection, Gas leakage quantification.

1. INTRODUCTION

The environmental safety and public health are becoming increasingly important in the industry. The emission of greenhouse gases is in particular a very serious issue. One of the possible mitigations to CO_2 emission is the storage of the gas in sub-seafloor reservoirs. Leakages from those reservoirs must be monitored, to ensure the effectiveness of CO_2 storage and avoid releasing the gas to the atmosphere. Moreover as the global warming concern increases, there is a need to better characterize gas release mechanisms and amplitudes from natural methane sources.

From the seafloor, gas escaping underwater originates from the migration of gas through the sediments and diffuses in the water column either as dissolved gas or as a free gas. In the latter case, this takes the form of bubbles with different sizes and spatial structures varying from small bubble streams to larger bubble clouds. The shape of the bubbles and their trajectories change randomly, increasing the difficulty of the characterization of the gas flares.

Gas leakage monitoring requires a multi-level concept: detection, verification and characterization. Usually, gas leakages are detected with periodic surveys by means of ship-mounted sonar methods covering large areas. The verification and characterization can be executed by inspecting anomalies using ROV (Remote Operated Vehicles)-based techniques or stationary autonomous monitoring devices. In the verification step, it is determined if the flare is really a gas leak, not other structure like a school of fishes. In the characterization step, properties like gas type, spatial distribution and leak rate are determined.

In the characterization/quantification step, the amount of data is normally less than in the detection phase, because only the parts that contain flares are considered. But the need for processing power and advanced algorithms is still very high. The automation of the processing is also important, because the number of flares and data blocks can be very high.

The literature on the gas leak quantification subject presents few studies but it is possible to mention some some studies using different techniques like optical (Ravikumar et al., 2016), sensors (Shitashima et al., 2015), acoustics (Berges et al., 2015; Muyakshin and Sauter, 2010) and ultrasound (Ostrovsky et al., 2008).

In this work, the characterization of a gas leakage by an optical method is analyzed and the results are then compared with another method using ultrasound measurements. The vertical speed and size of air bubbles in water and the gas flow rate are evaluated through images captured with a high-speed video camera. The paper has the following structure, Section 2 describes the leak quantification proposed algorithm. Two different methods are described: the optical and the ultrasound based methods. The optical

[1] This project was supported by Shell.
[2] e-mail: takimotoyugo@gmail.com
[3] e-mail: rsc@mym.eng.br
[4] e-mail: timoteolavras@gmail.com
[5] e-mail: jcadamow@usp.br
[6] e-mail: andre.sato@usp.br
[7] e-mail: thiago@usp.br
[8] e-mail: mtsuzuki@usp.br

method can process the case of bubbles with partial overlapping. Section 3 has the experiment description. Section 4 has the results and Section 5 has the conclusions.

2. LEAK QUANTIFICATION PROCESS

Two different methods are proposed herein. The optical method is described first. It is described the algorithm that can process bubbles with partial overlapping. In the following, the ultrasound based method is described.

2.1 Optical Method

Using a calibrated camera (Zhang, 2000), the real bubble size can be estimated from a captured image (see Fig. 1). From a video of a leakage, it is possible to extract each frame to evaluate the bubble size, the rise velocity and the flow rate.

The bubble size measurement using photographic techniques can use a simple approach that exploits the fact that a bubble in a liquid act like an inverse, spherical lens which creates a virtual image photographed by the camera. The relationship between the size of the final image and the imaged object is directly related to the curvature of the bubble and hence its radius.

A frequently used technique to evaluate the bubble size with optical photography determines the bubble cross sectional area A_{Proj} determined from the projected image. Then assuming that the bubbles are well approximated as ellipsoids (or more specifically an oblate spheroid), an equivalent bubble chord length

$$d = \sqrt{\frac{4bA_{Proj}}{\pi}} \tag{1}$$

can be computed. Here, b is the ratio between the large diameter and the small diameter (i.e., aspect ratio).

The first step after the video frame extraction to evaluate the bubble size is the bubble identification in each image. Therefore, each frame is processed and the bubble edges can be extracted (see Fig. 2). The edge detection can be performed by estimating the gradient magnitude using a convolutional filter (Sobel and Feldman, 1968) or a Gaussian filter (Canny, 1986). The Sobel uses a discrete differentiation operator to estimate the gradient in the x-direction and in the y-direction. This operator is very simple and can detect the edge orientation. However, there exist some disadvantages of the Sobel edge detector method: it is sensitive to noise. The magnitude of the edges degrades as the level of noise presented in the image increases. The Canny edge detector uses a filter based on the first derivative of a Gaussian filter and classifies a pixel as an edge if the gradient magnitude of the pixel is larger than those of pixels at both its sides in the direction of maximum intensity change. Although it consumes a lot of time due to its complex computation, it has a good signal strengthening with respect to the noise ratio and better detection of edges especially in noisy state by applying a threshold method.

In this work, these two detectors were tested to recover the bubble edges. The sectional area is evaluated after the bubble edge detection (see Fig. 3). Since the result of

Fig. 1. Captured image with bubbles.

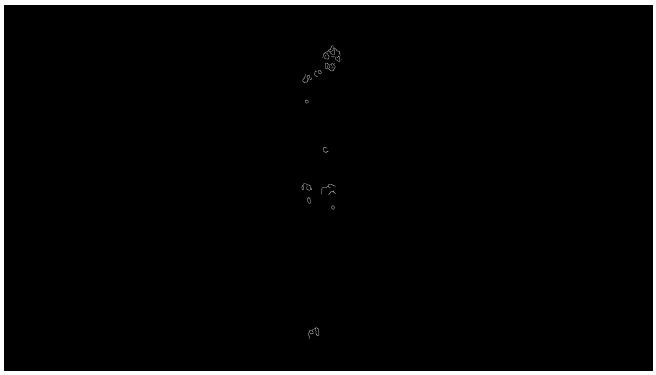

Fig. 2. Bubble contours extracted from the captured image.

edges detectors algorithms is a set of unconnected areas, to evaluate the sectional area it is necessary to obtain the connected contour. Among the algorithms to obtain the connected contour, it is possible to mention the Square Tracing Algorithm (Pratt, 2001) and the Moore-Neighbor Tracing (Sonka et al., 2007). The Square Tracing Algorithm is based on two rules: if the value of the active pixel is equal to one (the active pixel is at the point belonging the object), then the left turn; otherwise, when the active pixel value is zero (the active pixel is at a point, which does not belong the object), then the right turn. The Moore-Neighbor Tracing verifies all adjacent points in order to find the next contour point. The stopping criteria for both algorithms is the return to the starting point. After the contour recover, it is necessary to fill the holes inside the contour to evaluate the sectional area. The hole filling process can be executed through a morphological reconstruction. This morphological reconstruction analyses the contour connectivity to fill the holes. Once the bubble is completely identified, the bubble parameters can be extracted.

The sectional area is evaluated by analysing the image pixels and by calculating the white/black ratio.

Vertical velocity The bubble vertical velocity is evaluated by measuring the vertical displacement on the projected image between an image and the next one. The vertical velocity is calculated by this vertical offset divided by the difference of time between the two consective images.

Bubble volume Since the bubble diameter is evaluated from the cross sectional area given by equation (1) mea-

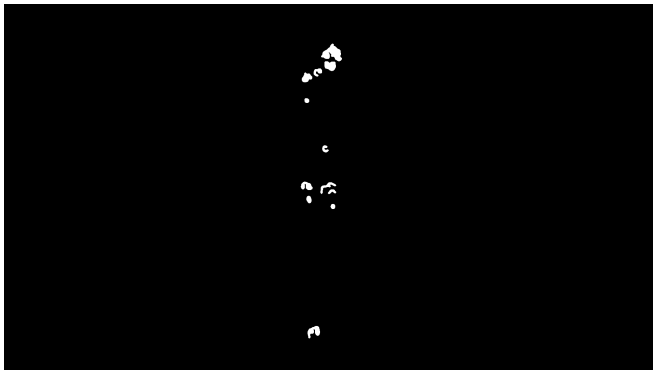

Fig. 3. Bubble sectional area recovery.

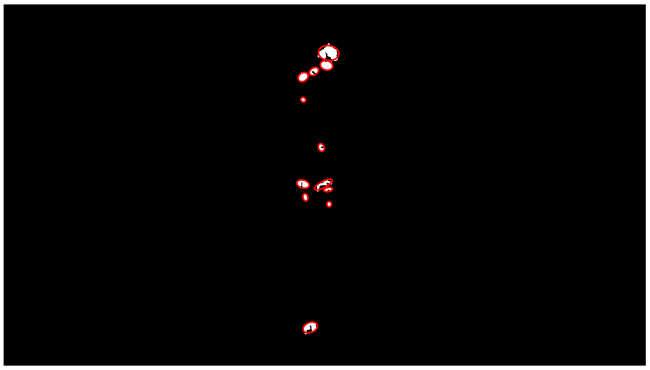

Fig. 4. Bubble ellipse approximation.

sured in each image and it was considered a spherical approximation for the captured bubbles, the bubble volume can be calculated using the evaluated bubble diameter.

Bubble rate The bubble rate is calculated by determining the number of frames required for the next bubble reaches the same vertical position. The calculation uses the difference of time between two consecutive images to obtain the rate at which bubbles are emitted.

Leak rate The leak rate is then calculated by the bubble rate multiplied by the bubble volume.

2.2 Bubble Partial Overlapping Consideration

Some initial tests were performed to capture the bubbles with the camera. The initial tests showed that as the bubble flow increases, the complexity of the bubble spatial distribution also increases and some bubble partial overlapping happens. To deal with this problem, an overlapping object recognition algorithm proposed by Honkanen et al. (2005) was implemented. This algorithm calculates the overall perimeter of a segment, finds the points at the perimeter that represent the connecting points of overlapping objects, clusters the perimeter arcs that belong to the same object and fits ellipses on the clustered arcs of the perimeter.

The Fig. 1 shows a frame of 1 min video with bubbles overlapping. The Fig. 5 shows the results comparing the bubble ellipsoid approximation using two different algorithms. The Fig. 5(c) uses the filled region for an ellipsoid approximation while the Fig. 5(d) uses the perimeter that represent the connecting points.

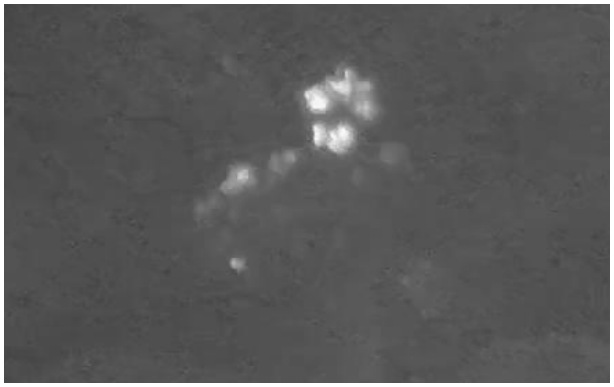

(a)

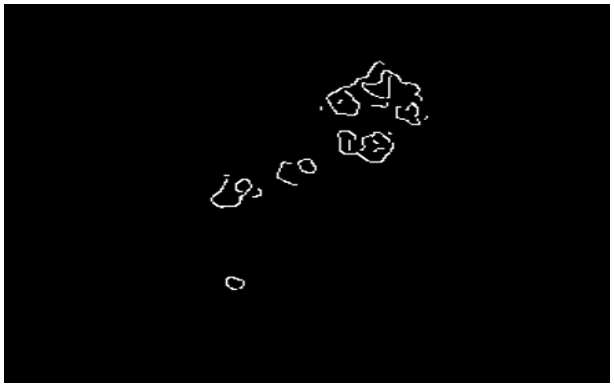

(b)

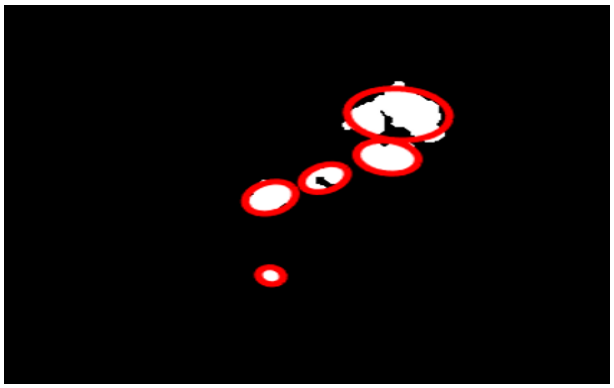

(c)

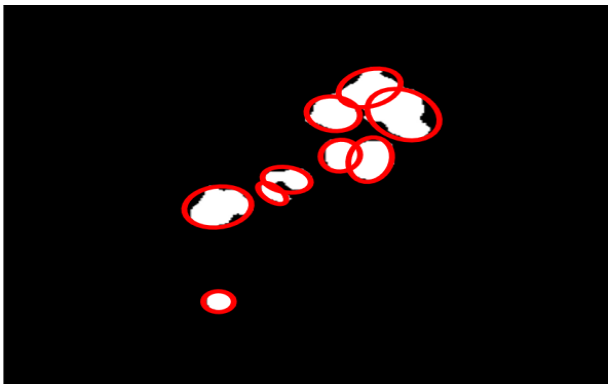

(d)

Fig. 5. Overlapping Algorithm Test.(a) Original Image. (b) Detect Borders. (c) Filled area ellipse approximation. (d) Bubble overlapping algorithm.

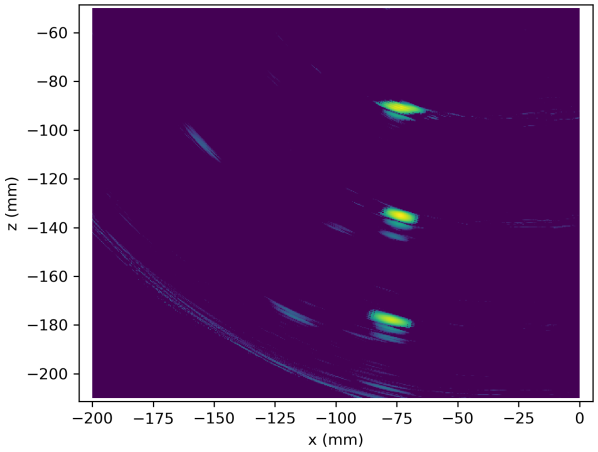

Fig. 6. Ultrasound image of bubbles.

The full video was analysed and the average radius considering the first method was 1.43 cm and for the second method the average radius was 1.54 cm. The leak rate was also evaluated using both methods. For the first method the leak rate was 98.44 ml/s and for the second method the leak rate was 122.38 ml/s.

2.3 Ultrasound Based Method

In this method, acoustic waves are produced and the echo is received by array transducers (Adamowski et al., 2013), forming images like in Fig. 6. Contrary to the optical method, the ultrasound images do not show the bubble edges, they show an echo over the leading surface of the bubble, from the point of view of the transducer. Since the ultrasound measurement cannot detect the bubble shape, it depends on statistics to obtain an approximation of the correct values.

Vertical velocity: The vertical velocity of the bubbles is measured using a 2D cross-correlation between an image and the next one. The 2D processing is done to adapt to small horizontal movements. In the resulting 2D data, only the vertical offset of the peak is considered. The vertical velocity is calculated by the vertical offset divided by the time between images.

Bubble volume: To calculate the bubble volume from the vertical velocity, experimental data can be utilized, such as provided by Kulkarni and Joshi (2005) and Ostrovsky et al. (2008). The importance of the experimental data is that they are obtained using non-spherical bubbles, because in experiments it is extremely difficult to generate and maintain spherical gas bubbles in water. In this work, the curves in Fig. 7 are utilized. The curves provide the terminal vertical velocity for each bubble size, which is indicated by the radius of a sphere with the same volume. The problem with the curve is that it is not invertible. To be able to use this curve, in this work only radii above 0.42 cm are considered.

Bubble rate: The bubble rate is calculated using 2D autocorrelation, when there are more than one bubble in each image. In the case when there is only one bubble in each image, 2D cross-correlation between images containing consecutive bubbles is utilized. The calculation uses the measured vertical offset, vertical speed and time between

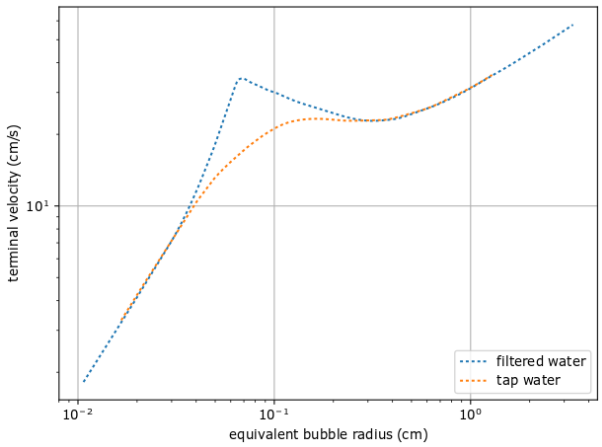

Fig. 7. Terminal velocity of single air bubbles obtained experimentally, in filtered and tap water. The water temperature is around 20^o. Adapted from (Haberman and Morton, 1953).

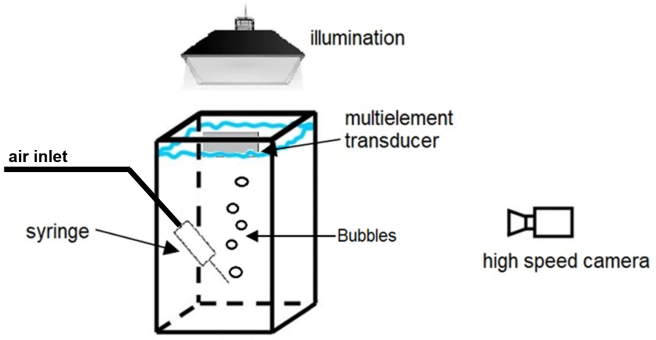

Fig. 8. Experiment diagram.

images (in the case of one bubble per image) to obtain the rate at which bubbles are emitted.

Leak rate: Finally the leak rate is calculated by the bubble rate multiplied by the bubble volume.

3. EXPERIMENTS

The experimental setup of Fig. 8 was used for the leak quantification. In this setup, air bubbles were injected in the liquid medium by a syringe connected to an air inlet (compressor air pump). Bubbles of different sizes were generated by controlling the air flow rate. Images of the rising bubbles were captured by a high speed camera and by the multielement ultrasonic transducer.

3.1 Optical bubble measurement

Images of the bubbles were captured using a Fastec (USA) InLine IN1000M1GB high-speed camera at 1000 fps. In this approach, due to the reduced exposure, a high intensity light is required to illuminate the scene. Flicker in images is another issue to be addressed in high speed capture. The flicker is caused by the constant fluctuation of room light due to the alternating current (AC) at a power line frequency of 60 Hz or 50 Hz, depending on the country. For this experiment, a special illumination with LEDs was

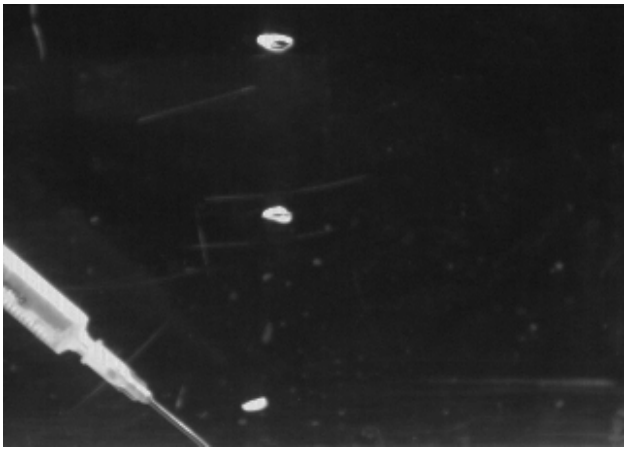

Fig. 9. Optical image of bubbles.

Fig. 10. Processed image.

prepared to provide enough illumination to capture the bubbles and to prevent the flicker effect.

Although the experimental setup used an alternating current power source, with a proper cooling system design a high power led flashlight can be achieved with a DC power source for a underwater quantification. Moreover the ROV arm can be used to properly adjust the illumination position and also some additional techniques can be used to enhance the image quality (Garcia et al., 2002).

For each leak rate a video with 18396 frames were acquired by the camera.

The Fig. 9 shows the image captured with the high speed camera. Using some image processing techniques, it was possible to remove the image background, recover the approximated bubble ellipsoids and evaluate the bubble parameters (see Fig. 10).

The vertical speed is not necessary for the calculation of leak rate in the optical method, but it is obtained to allow the comparison with the ultrasonic method.

3.2 Ultrasound bubble measurement

Ultrasound images of the bubbles were captured using a Sitau 32:128MX acquisition device from Dasel (Spain), with 32 channels multiplexed in 128. This device is designed for nondestructive testing (NDT). An ultrasound linear array from Imasonic (France) with 500 kHz center frequency was utilized, with pitch of 1.5 mm and 64 elements. Only the first 32 elements were active in the experiments.

Table 1. Leak measurements.

Case	Vertical speed (cm/s)	Equivalent bubble radius (cm)	Bubble rate (Hz)	Leak rate (ml/s)
Optical				
1	24.1	0.536	1.524	0.98
2	26.8	0.618	4.219	4.18
3	27.1	0.736	7.142	11.92
Ultrasound				
1	24.5	0.511	1.503	0.84
2	26.5	0.663	4.138	5.05
3	27.6	0.746	6.408	11.13

A common sonar transducer shape is the Mills Cross, resembling a "T". To roughly reproduce the behaviour of this type of transducer, the set of active elements emitted a divergent wave front, with focal point 5 cm behind the frontal face of the transducer ($z_\mathrm{F} = -5\,\mathrm{cm}$), and all the active elements were used in reception. The transmit delays for each array element i are given by $\Delta t_i = \Delta t_{\mathrm{F}i} - \min_i \Delta t_{\mathrm{F}i}$, where $\Delta t_{\mathrm{F}i} = \sqrt{(x_i - x_\mathrm{F})^2 + z_\mathrm{F}^2}/c$, the element centers are at $x = x_i$, $y = 0$ and $z = 0$, the focal point is at $x = x_\mathrm{F}$, $y = 0$ and $z = z_\mathrm{F}$, and c is the sound speed in water. The image value at point P is obtained by

$$I_\mathrm{P} = \sum_j s_j(t_{\mathrm{P}j}) \tag{2}$$

where s_j is the acoustic signal received by the element j, $t_{\mathrm{P}j} = \sqrt{(x_\mathrm{P} - x_\mathrm{F})^2 + (z_\mathrm{P} - z_\mathrm{F})^2}/c - \min_i \Delta t_{\mathrm{F}i} + \sqrt{(x_\mathrm{P} - x_j)^2 + z_\mathrm{P}^2}/c$ is the travel time and the point P is at $x = x_\mathrm{P}$, $y = 0$ and $z = z_\mathrm{P}$.

For each leak rate case, 100 acquisitions were captured, each one producing an image. The time between acquisitions was 100 ms, which is the round trip travel time in water for a distance of 75 m.

4. RESULTS

The results, shown in Table 1, have been calculated by the average of the results for the many captured images. The maximum errors between the optical and ultrasound methods were 1.8 % for vertical speed, 4.9 % for equivalent bubble radius, 11 % for bubble rate and 21 % for leak rate.

The larger error in the leak rate can be explained by its formula, which depends on r^3, where r is the equivalent bubble radius, and on the bubble rate. For example, an error of 1 % in the radius plus an error of 1 % in the bubble rate produce an error of 4 % in the leak rate.

5. CONCLUSION

The errors between the results of the optical and ultrasound methods can be considered acceptable if the limitations of the utilized methods are considered. The optical method uses a 2D projection of the 3D shape of the bubble, while the ultrasound method does not even have access to the 2D projection of the bubble. On the other hand,

ultrasound (sonar) can be used to measure the bubbles from a distance of tens of meters or more, even when the water is not clear.

The leak quantification using optical and sonar technologies involves multiple steps, requiring a careful methodology to integrate the many components.

The effect of error accumulation due to multiple steps in the calculation has been observed, and may become a challenge if an accurate measurement is needed.

For the future work undersea tests are required to verify the use of the proposed method in limited visibility due to suspended particles, in high water pressure and in different ocean currents.

ACKNOWLEDGEMENTS

We gratefully acknowledge support of the RCGI Research Centre for Gas Innovation, hosted by the University of São Paulo (USP) and sponsored by FAPESP São Paulo Research Foundation (2014/50279-4) and Shell Brasil, and the strategic importance of the support given by ANP (Brazil's National Oil, Natural Gas and Biofuels Agency) through the R&D levy regulation. R. Y. Takimoto, M. Y. Matuda and T. F. Oliveira were supported by FUSP/Shell. M. S. G. Tsuzuki and J. C. Adamowski were partially supported by CNPq (proc. 305959/2016–6 and 311.195/2019-9).

REFERENCES

Adamowski, J.C., Buiochi, F., Tsuzuki, M.S.G., Pérez, N., Camerini, C.S., and Patusco, C. (2013). Ultrasonic measurement of micrometric wall-thickness loss due to corrosion inside pipes. In *IEEE International Ultrasonics Symposium (IUS)*, 1881–1884.

Berges, B., Leighton, T., and White, P. (2015). Passive acoustic quantification of gas fluxes during controlled gas release experiments. *International Journal of Greenhouse Gas Control*, 38, 64–79.

Canny, J. (1986). A computational approach to edge detection. *IEEE T Pattern Anal*, 8(6), 679–698.

Garcia, R., Nicosevici, T., and Cufi, X. (2002). On the way to solve lighting problems in underwater imaging. In *OCEANS '02 MTS/IEEE*, volume 2, 1018–1024 vol.2.

Haberman, W.L. and Morton, R.K. (1953). An experimental investigation of the drag and shape of air bubbles rising in various liquids. Technical report, The David W. Taylor Model Basin.

Honkanen, M., Saarenrinne, P., Stoor, T., and Niinimaki, J. (2005). Recognition of highly overlapping ellipse-like bubble images. *Meas Sci Technol*, 16(9), 1760–1770.

Kulkarni, A.A. and Joshi, J.B. (2005). Bubble formation and bubble rise velocity in gas-liquid systems: A review. *Ind Eng Chem Res*, 44(16), 5873–5931.

Muyakshin, S. and Sauter, E. (2010). The hydroacoustic method for the quantification of the gas flux from a submersed bubble plume. *Oceanology*, 50, 995–1001.

Ostrovsky, I., McGinnis, D.F., Lapidus, L., and Eckert, W. (2008). Quantifying gas ebullition with echosounder: the role of methane transport by bubbles in a medium-sized lake. *Limnol Oceanogr-Meth*, 6(2), 105–118.

Pratt, W.K. (2001). *Digital Image Processing: PIKS Inside*. John Wiley & Sons, Inc., New York, NY, USA, 3rd edition.

Ravikumar, A., Wang, J., and Brandt, A. (2016). Are optical gas imaging technologies effective for methane leak detection? *Environmental Science & Technology*, 51.

Shitashima, K., Maeda, Y., and Sakamoto, A. (2015). Detection and monitoring of leaked co2 through sediment, water column and atmosphere in a sub-seabed ccs experiment. *International Journal of Greenhouse Gas Control*, 38.

Sobel, I. and Feldman, G. (1968). A 3x3 Isotropic Gradient Operator for Image Processing. Never published but presented at a talk at the Stanford Artificial Project.

Sonka, M., Hlavac, V., and Boyle, R. (2007). *Image Processing, Analysis, and Machine Vision*. Thomson-Engineering.

Zhang, Z. (2000). A flexible new technique for camera calibration. *IEEE T Pattern Anal*, 22(11), 1330–1334.